

Supporting Information

Derivatives of 2-(3,4-dinitro-1*H*-pyrazol-1-yl) acetonitrile:

**Design strategy, syntheses, and properties of a series of new
melt-cast explosives**

Tongwei Zhang, Xiaofeng Yuan, Ze Xu, Ming Lu,* Yuangang Xu*

School of Chemistry and Chemical Engineering, Nanjing University of Science and
Technology, Xiaolingwei 200, Nanjing 210094, China.

* Corresponding authors: luming302@126.com, yuangangxu@163.com

Table of contents

I. General remarks.....	s3
II . Crystal data	s4
III. Calculation of heats of formation.....	s10
IV. References.....	s12
V . Copies of NMR spectra.....	s13

I. General remarks

General methods: Unless otherwise noted, all reagents were obtained from commercial suppliers and used without further purification. NMR spectra were obtained on a Bruker AVANCE III 500 spectrometer. The ¹H NMR (500 MHz) chemical shifts were measured relative to DMSO-*d*₆ as the internal reference (DMSO-*d*₆: δ = 2.50 ppm). The ¹³C NMR (125.72 MHz) chemical shifts were given using DMSO-*d*₆ as the internal standard (DMSO-*d*₆: δ = 39.52 ppm). Infrared (IR) spectra were recorded on a Perkin-Elmer Spectrum II IR Spectrometers using KBr pellets. X-Ray single-crystal diffraction data were collected on a Rigaku AFC-10/Saturn 724+CCD diffractometer with graphite-monochromated Mo K α radiation (λ =0.71073 Å) using the multi-scan technique. Thermal decomposition temperatures were determined by using differential scanning calorimetry (DSC) on a Mettler-Toledo TGA/DSC 1 Stare system at a heating rate of 5 °C·min⁻¹ from room temperature to 400 °C under nitrogen atmosphere. The detonation parameters, including detonation velocity and detonation pressure, were calculated by using the EXPLO5 (version 6.05.04) program. The impact and friction sensitivities were measured on a standard BAM fall hammer and a BAM friction tester¹. Hirshfeld surfaces and 2D fingerprint plots were generated by CrystalExplorer (version 17.5)². The electrostatic potential (ESP) surfaces and non-covalent interaction (NCI) analyses were analyzed and drawn by using Multiwfn (version 3.5)³ and Visual Molecular Dynamics (VMD, version 1.9.3) program suites.

II. Crystal data

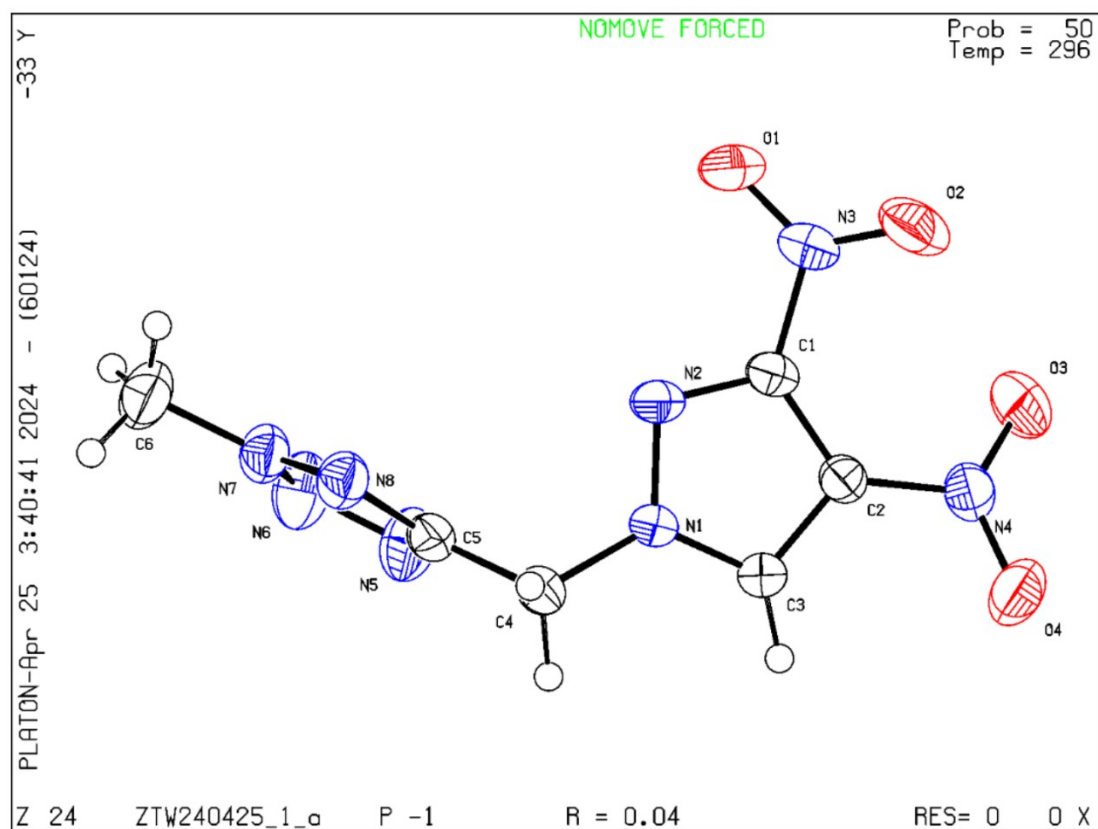


Figure S1. ORTEP diagram of compound **4** at room temperature. Thermal ellipsoids are shown at the 50% probability level

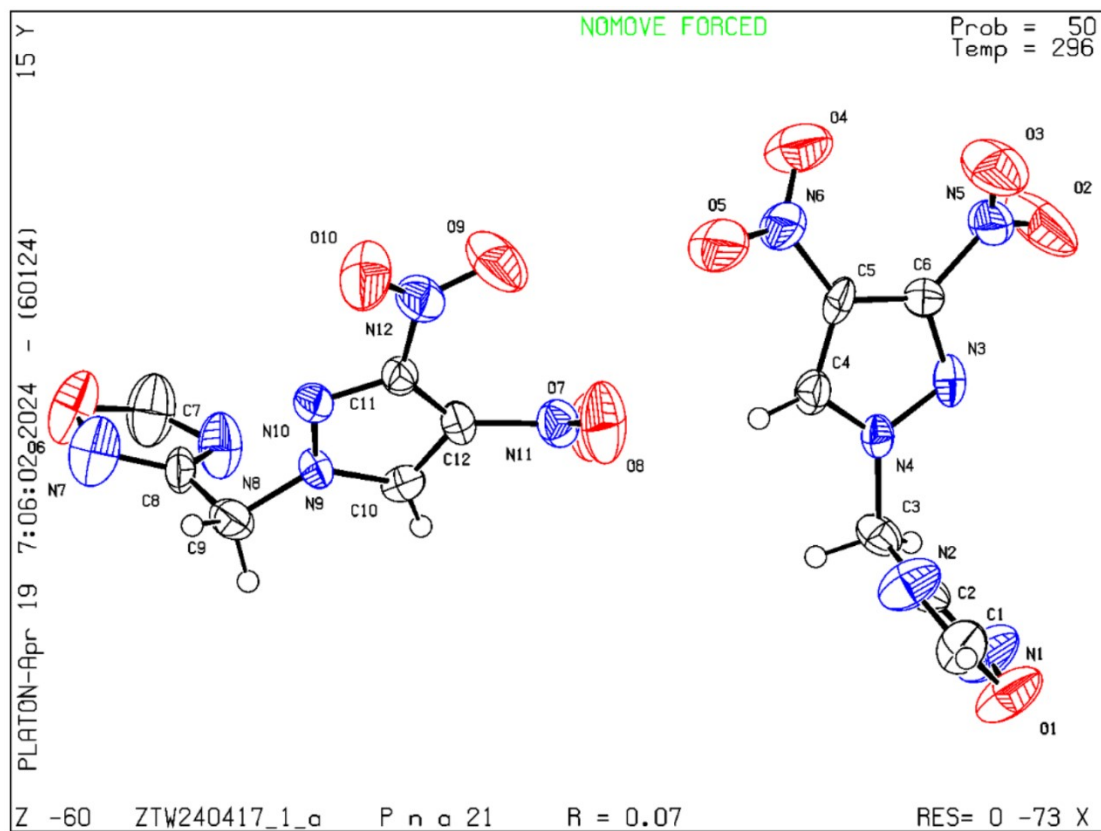


Figure S2. ORTEP diagram of compound **6** at room temperature. Thermal ellipsoids are shown at the 50% probability level

Volume/ \AA^3	508.71(4)
Z	2
ρ_{calc} g/m ³	1.659
μ/mm^{-1}	0.141
F(000)	260
Crystal size/mm ³	0.120 x 0.100 x 0.090
2 Θ range for data collection/°	2.931 to 27.483
Index ranges	-8<=h<=8, -9<=k<=9, -14<=l<=14
Reflections collected	7846
Independent reflections	2314 [R(int) = 0.0241]
Data / restraints / parameters	2314 / 0 / 164
Goodness-of-fit on F ²	1.033
Final R indices [I>2sigma(I)]	R1 = 0.0423, wR2 = 0.1020
Final R indices (all data)	R1 = 0.0570, wR2 = 0.1104
Largest diff. peak and hole/ e. \AA^{-3}	0.239 and -0.239

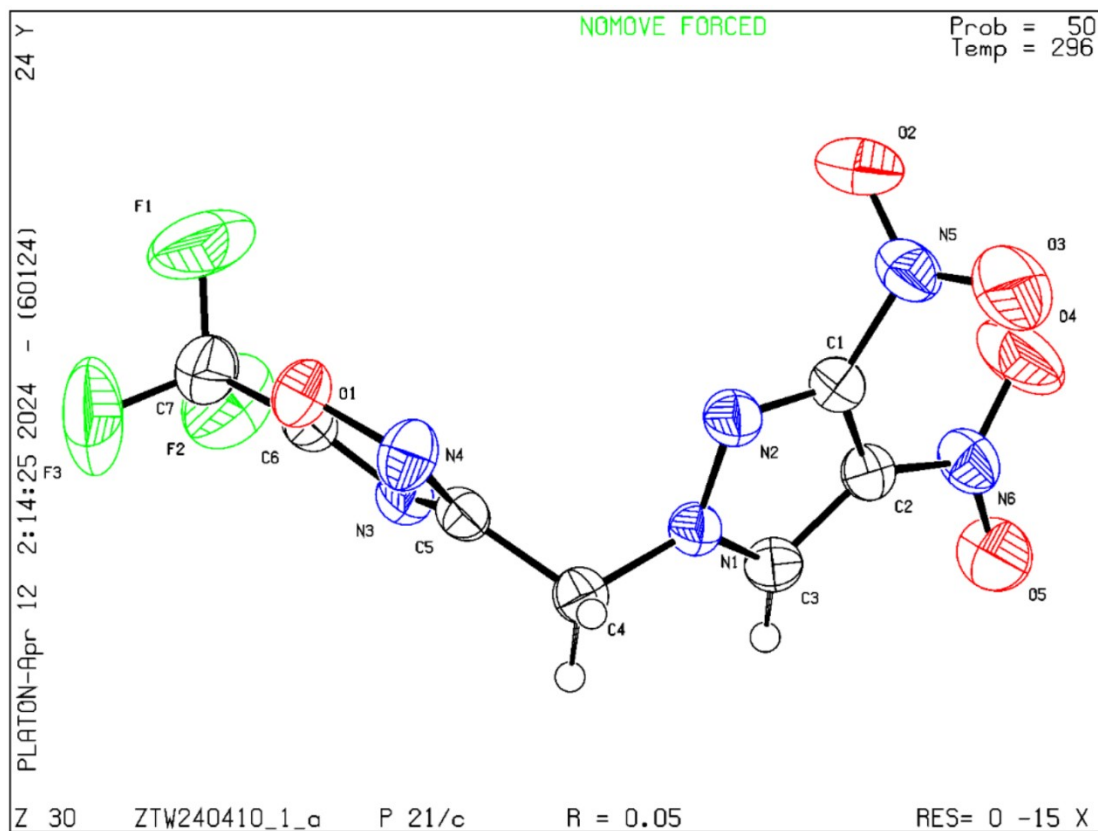


Figure S3. ORTEP diagram of compound **7** at room temperature. Thermal ellipsoids are shown at the 50% probability level

Volume/ \AA^3	508.71(4)
Z	2
ρ_{calc} g/m ³	1.659
μ/mm^{-1}	0.141
F(000)	260
Crystal size/mm ³	0.120 x 0.100 x 0.090
2 Θ range for data collection/°	2.931 to 27.483
Index ranges	-8<=h<=8, -9<=k<=9, -14<=l<=14
Reflections collected	7846
Independent reflections	2314 [R(int) = 0.0241]
Data / restraints / parameters	2314 / 0 / 164
Goodness-of-fit on F ²	1.033
Final R indices [I>2sigma(I)]	R1 = 0.0423, wR2 = 0.1020
Final R indices (all data)	R1 = 0.0570, wR2 = 0.1104
Largest diff. peak and hole/ e. \AA^{-3}	0.239 and -0.239

Table S1. Crystal data for compound **4** at room temperature

Identification code	4
CCDC number	2379758
Empirical formula	C ₆ H ₆ N ₈ O ₄
Formula weight	254.19
Temperature/K	296(2)
Crystal system	Triclinic
Space group	P-1
a/ \AA	6.7014(3)
b/ \AA	7.4750(4)
c/ \AA	11.2966(5)
$\alpha/^\circ$	97.876(2)
$\beta/^\circ$	104.754(2)
$\gamma/^\circ$	107.211(2)

Table S2. Crystal data for compound **6** at room temperature

Identification code	6
CCDC number	2379757
Empirical formula	C ₆ H ₄ N ₆ O ₅
Formula weight	240.15
Temperature/K	296(2)
Crystal system	Orthorhombic
Space group	Pna2 ₁
a/Å	15.229(5)
b/Å	5.3345(15)
c/Å	23.556(6)
α/°	90
β/°	90
γ/°	90
Volume/Å ³	1913.7(10)
Z	8
ρ _{calc} g/m ³	1.667
μ/mm ⁻¹	0.147
F(000)	976
Crystal size/mm ³	0.180 x 0.160 x 0.120
2Θ range for data collection/°	2.675 to 27.563
Index ranges	-19<=h<=18, -6<=k<=6, -30<=l<=26
Reflections collected	13949
Independent reflections	4058 [R(int) = 0.0761]
Data / restraints / parameters	4058 / 1 / 307
Goodness-of-fit on F ²	1.034
Final R indices [I>2sigma(I)]	R1 = 0.0651, wR2 = 0.1354
Final R indices (all data)	R1 = 0.1356, wR2 = 0.1572
Largest diff. peak and hole/ e.Å ⁻³	0.266 and -0.213

Table S3. Crystal data for compound **7** at room temperature

Identification code	7
CCDC number	2379760
Empirical formula	C ₇ H ₃ F ₃ N ₆ O ₅
Formula weight	308.15
Temperature	296(2)
Crystal system	Monoclinic
Space group	P2 ₁ /c
a/Å	8.8436(5)
b/Å	8.0309(5)
c/Å	15.9838(10)
α/°	90
β/°	95.681(2)
γ/°	90
Volume/Å ³	1129.63(12)
Z	4
ρ _{calc} g/m ³	1.812
μ/mm ⁻¹	0.183
F(000)	616
Crystal size/mm ³	0.200 x 0.180 x 0.080
2Θ range for data collection/°	2.314 to 27.516
Index ranges	-11<=h<=11, -8<=k<=10, -19<=l<=20
Reflections collected	11013
Independent reflections	2584 [R(int) = 0.0327]
Data / restraints / parameters	2584 / 0 / 191
Goodness-of-fit on F ²	1.030
Final R indices [I>2sigma(I)]	R1 = 0.0496, wR2 = 0.1401
Final R indices (all data)	R1 = 0.0824, wR2 = 0.1329
Largest diff. peak and hole/ e.Å ⁻³	0.427 and -0.418

III. Calculation of heats of formation

Computations were performed by using the *Gaussian 09* suite of programs.⁴ The elementary geometric optimization and the frequency analysis were performed at the level of the Becke three parameter, Lee-Yan-Parr (B3LYP)⁵ functional with the 6-311++G** basis set.⁶ All of the optimized structures were characterized to be local energy minima on the potential surface without any imaginary frequencies. Atomization energies were calculated by the CBS-4M.⁷ All the optimized structures were characterized to be true local energy minima on the potential-energy surface without imaginary frequencies.

The predictions of heats of formation (HOF) of compounds used the hybrid DFT-B3LYP methods with the 6-311++G** basis set through designed isodesmic reactions. The isodesmic reaction processes, that is, the number of each kind of formal bond is conserved, were used with the application of the bond separation reaction (BSR) rules. The molecule was broken down into a set of two heavy-atom molecules containing the same component bonds. The solid phase of heat of formation can be calculated according to the equation 1.

$$\Delta H_{solid} = \Delta H_{gas} - \Delta H_{sub} \quad (1)$$

Here, the heat of sublimation (ΔH_{sub}) was calculated by using an equation (2) proposed by Edward F. C. Byrd, et al.

$$\Delta H_{sub} = aA^2 + b(v\sigma_{tot}^2)^{1/2} + c \quad (2)$$

For all the ionic salts, calculation of the HOFs was simplified by using equation (3)

$$\Delta H(ionic\ salts, 298K) = \Sigma \Delta H(cation, 298K) + \Sigma \Delta H(anion, 298K) - \Delta H_L \quad (3)$$

In eq 3, ΔH_L is the lattice energy of the ionic salts, which could be predicted by using the equation (4) suggested by Jenkins et al.⁵

$$\Delta H_L = U_{POT} + [p(n_M/2 - 2) + q(n_X/2-2)]RT \quad (4)$$

In eq 4, n_M and n_X depended on the nature of ions M_p^+ and X_q^- , respectively, and are equal to 3 for monatomic ions, 5 for linear polyatomic ions, and 6 for nonlinear polyatomic ions.

The lattice-potential energy (U_{POT}) was calculated according to equation (5), in which ρ_m is the density (in g/cm³) and M_m is the chemical formula mass of the ionic material; the coefficients γ and δ were taken from the literature.⁸

$$U_{POT} (\text{kJ/mol}) = \gamma (\rho_m/M_m)^{1/3} - \delta \quad (5)$$

IV. References

1. United Nations. Recommendations on the transport of dangerous goods [M]. Manual of tests and criteria, 6th, United Nations Publication, New York, **2015**: 79-127.
2. Turner, M. J.; McKinnon, J. J.; Wolff, S. K.; Grimwood, D. J.; Spackman, P. R.; Jayatilaka, D.; Spackman, M. A. CrystalExplorer17 (2017). University of Western Australia. <http://hirshfeldsurface.net>
3. Lu T.; Chen, F. Multiwfn: A Multifunctional Wavefunction Analyzer. *J. Comput. Chem.* **2012**, 33, 580-592.
4. Frisch, M. J.; Trucks, G. W.; Schlegel, H. B.; Scuseria, G. E.; Robb, M. A.; Cheeseman, J. R.; Scalmani, G.; Barone, V.; Mennucci, B.; Petersson, G. A.; Nakatsuji, H.; Caricato, M.; Li, X.; Hratchian, H. P.; Izmaylov, A. F.; Bloino, J.; Zheng, G.; Sonnenberg, J. L.; Hada, M.; Ehara, M.; Toyota, K.; Fukuda, R.; Hasegawa, J.; Ishida, M.; Nakajima, T.; Honda, Y.; Kitao, O.; Nakai, H.; Vreven, T.; Montgomery, J. A.; Peralta, J. E.; Ogliaro, F.; Bearpark, M.; Heyd, J. J.; Brothers, E.; Kudin, K. N.; Staroverov, V. N.; Kobayashi, R.; Normand, J.; Raghavachari, K.; Rendell, A.; Burant, J. C.; Iyengar, S. S.; Tomasi, J.; Cossi, M.; Rega, N.; Millam, J. M.; Klene, M.; Knox, J. E.; Cross, J. B.; Bakken, V.; Adamo, C.; Jaramillo, J.; Gomperts, R.; Stratmann, R. E.; Yazyev, O.; Austin, A. J.; Cammi, R.; Pomelli, C.; Ochterski, J. W.; Martin, R. L.; Morokuma, K.; Zakrzewski, V. G.; Voth, G. A.; Salvador, P.; Dannenberg, J. J.; Dapprich, S.; Daniels, A. D.; Farkas, O.; Foresman, J. B.; Ortiz, J. V.; Cioslowski, J.; Fox, D. J.; Gaussian 09, Revision A.1; Gaussian, Inc.: Wallingford CT, 2009.
5. (a) Becke, A. D. Density - Functional Thermochemistry. III. The Role of Exact Exchange. *J. Chem. Phys.* **1993**, 98, 5648– 5652; (b) Stephens, P. J.; Devlin, F. J.; Chabalowski, C. F.; Frisch, M. J. Ab Initio Calculation of Vibrational Absorption and Circular Dichroism Spectra Using Density Functional Force Fields *J. Phys. Chem.* **1994**, 98, 11623– 11627.
6. Hariharan, P. C.; Pople J. A. The Influence of Polarization Functions on Molecular

- Orbital Hydrogenation Energies. *Theor. Chim. Acta*. **1973**, *28*, 213– 222.
7. Ochterski, J. W.; Petersson, G. A.; Montgomery, J. A. A Complete Basis Set Model Chemistry. V. Extensions to Six or More Heavy Atoms. *J. Chem. Phys.* **1996**, *104*, 2598– 2619.
8. (a) Jenkins, H. D. B.; Tudela, D.; Glasser, L. Lattice Potential Energy Estimation for Complex Ionic Salts from Density Measurements. *Inorg. Chem.* **2002**, *41*, 2364– 2367; (b) Jenkins, H. D. B.; Roobottom, H. K.; Passmore, J.; Glasser, L. Relationships among Ionic Lattice Energies, Molecular (Formula Unit) Volumes, and Thermochemical Radii. *Inorg. Chem.* **1999**, *38*, 3609– 3620.

V. Copies of NMR spectra

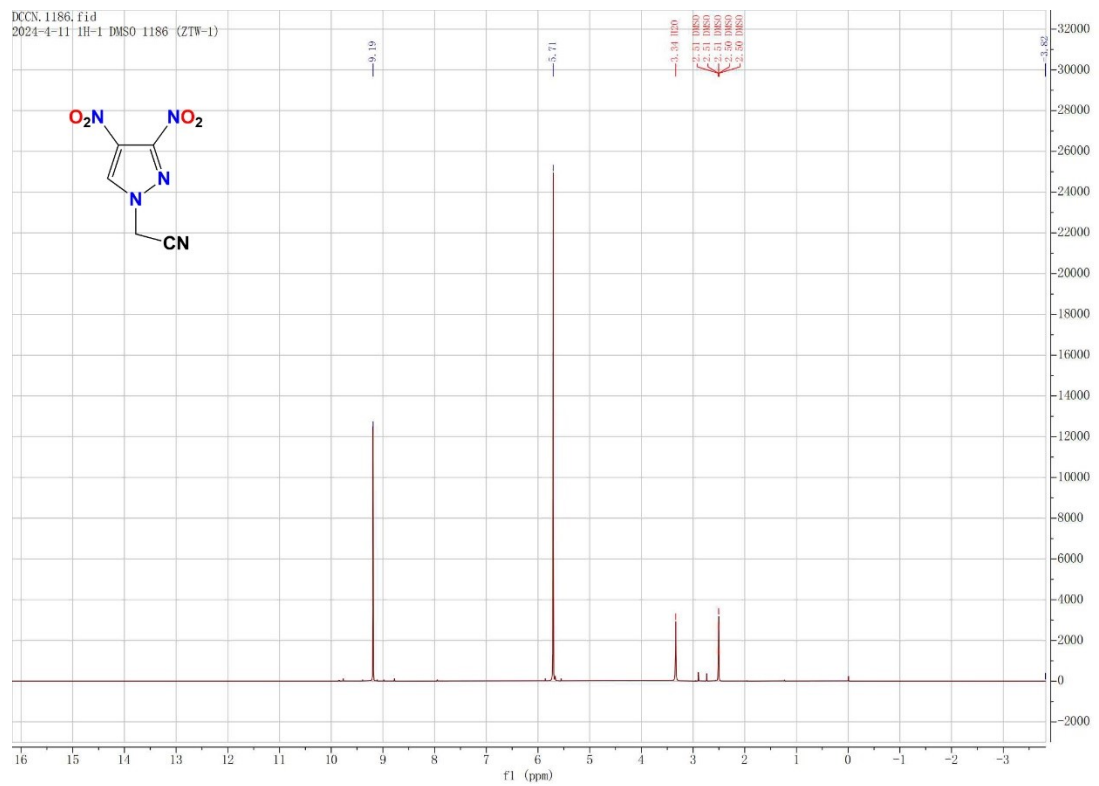


Figure S4. ^1H NMR spectrum in $\text{DMSO}-d_6$ for compound 2

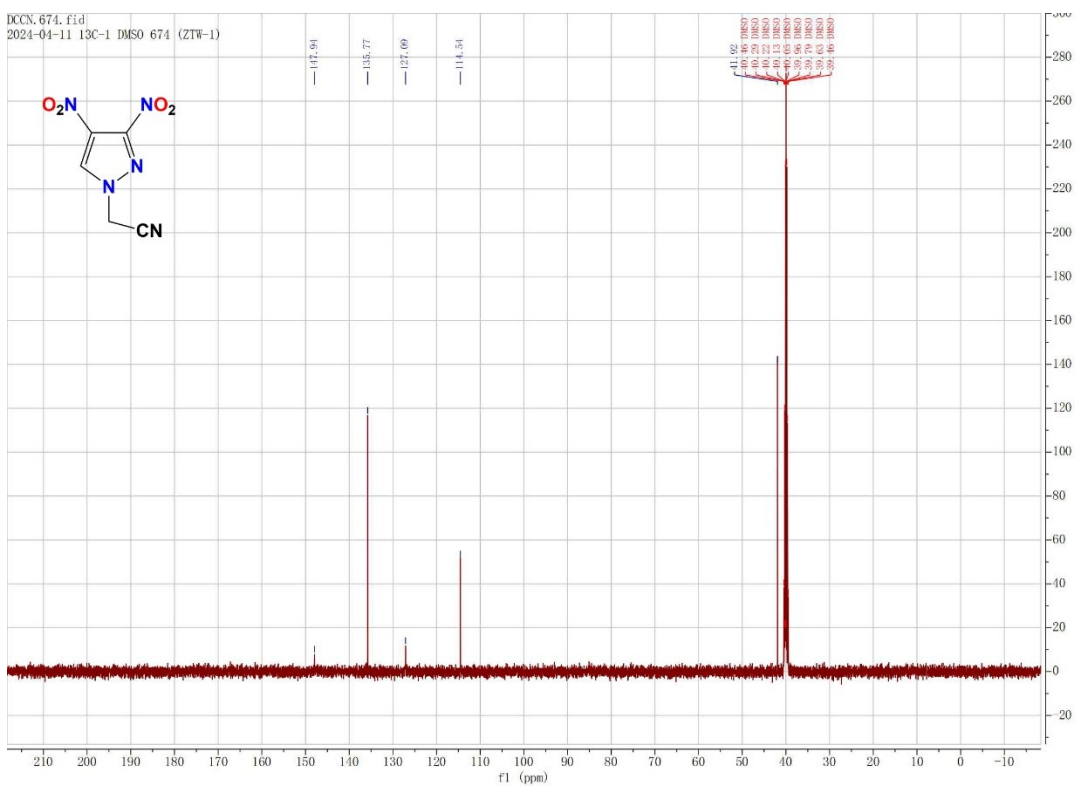


Figure S5. ^{13}C NMR spectrum in $\text{DMSO}-d_6$ for compound 2

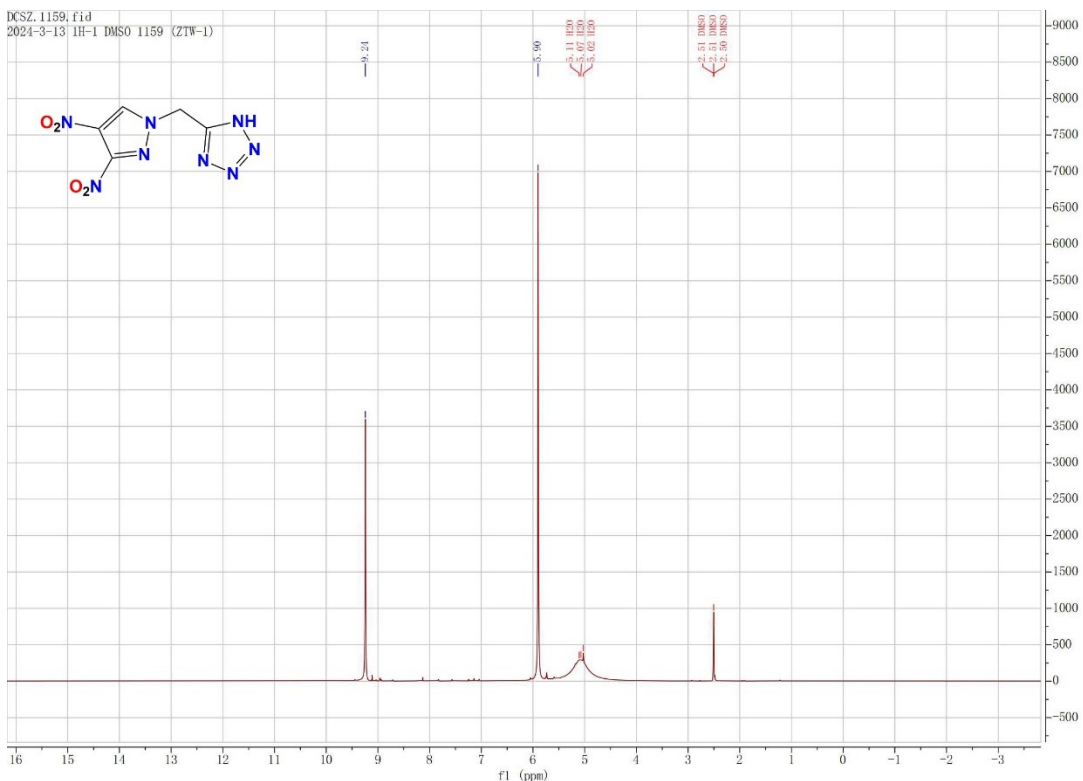


Figure S6. ^1H NMR spectrum in $\text{DMSO}-d_6$ for compound 3

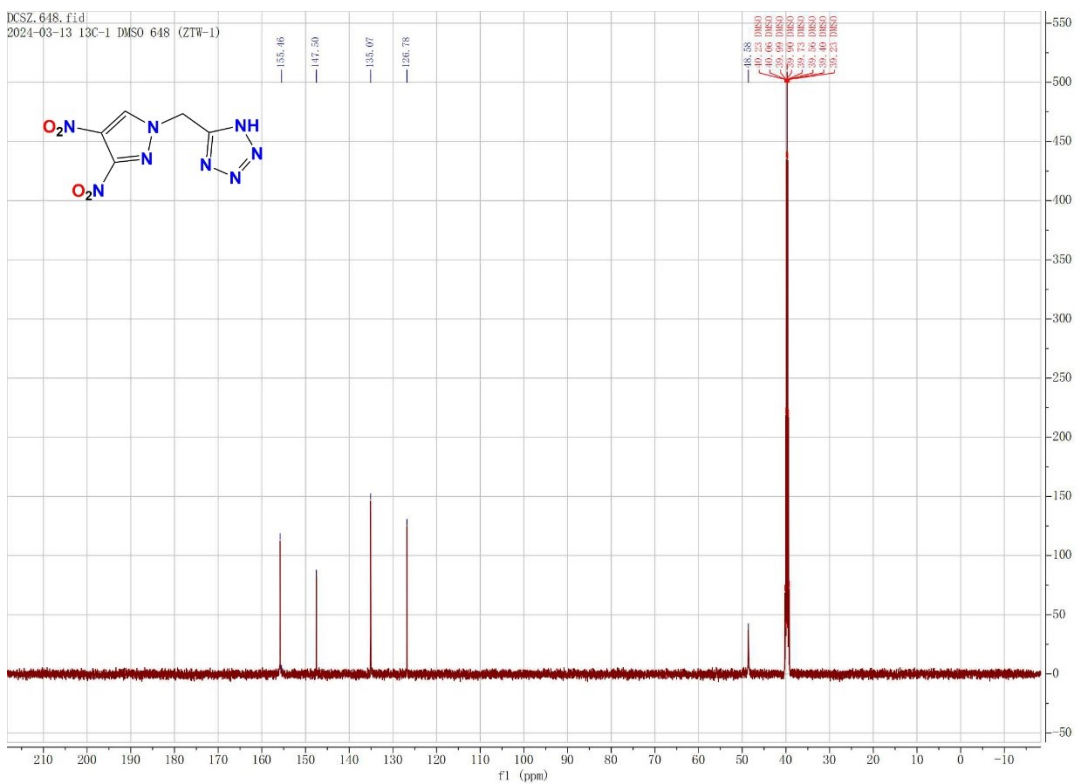


Figure S7. ^{13}C NMR spectrum in $\text{DMSO}-d_6$ for compound 3

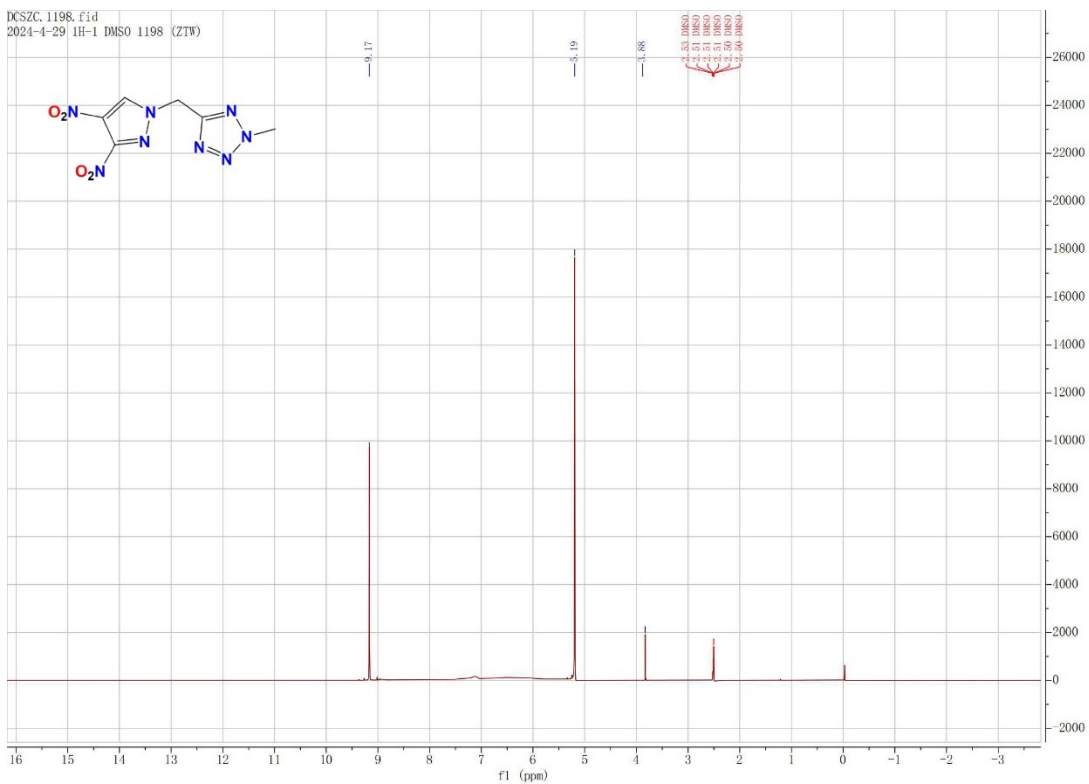


Figure S8. ^1H NMR spectrum in $\text{DMSO}-d_6$ for compound 4

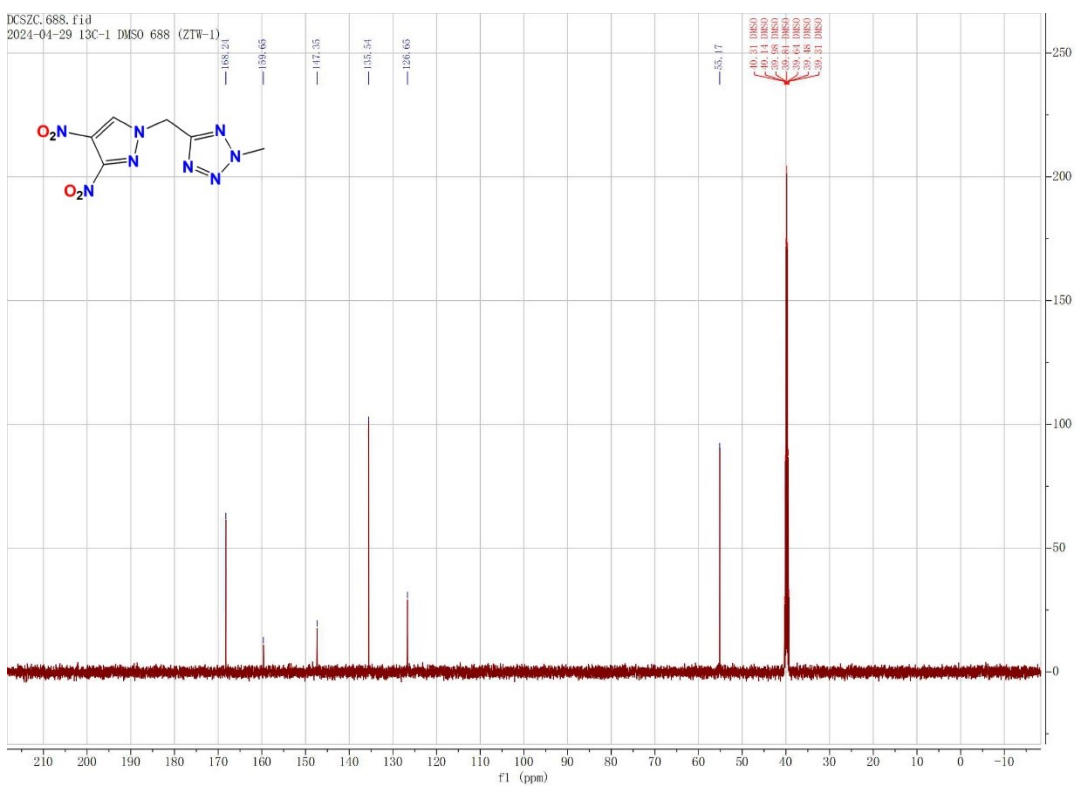


Figure S9. ^{13}C NMR spectrum in $\text{DMSO}-d_6$ for compound 4

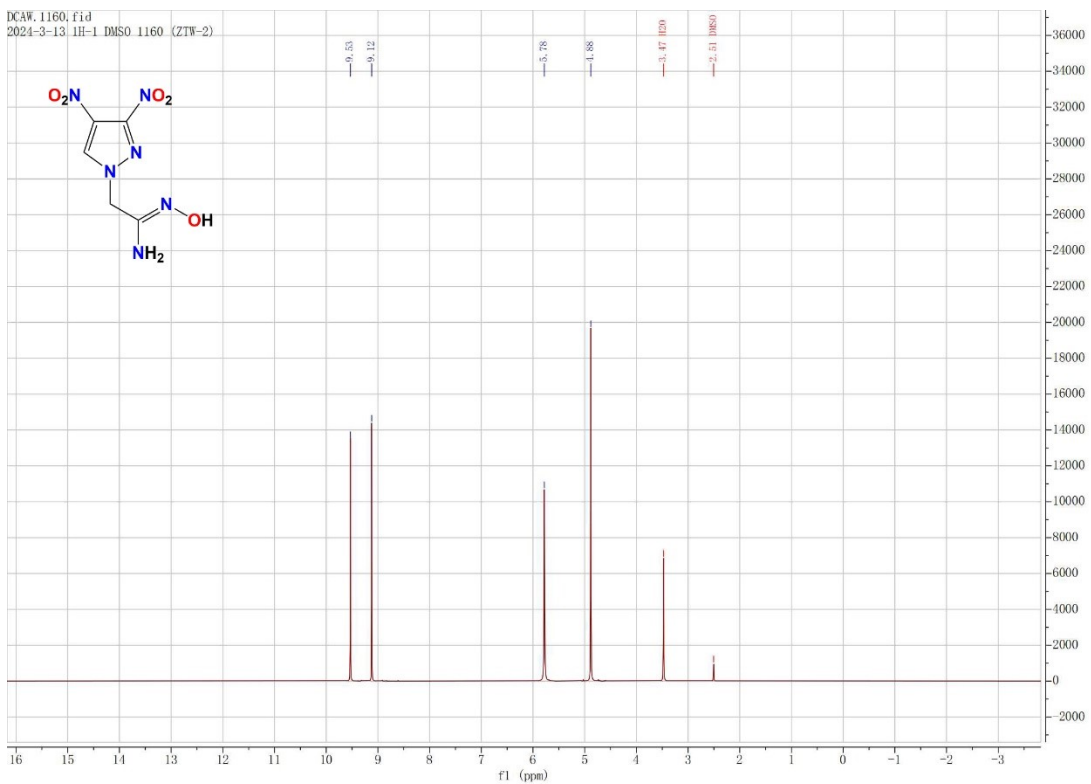


Figure S10. ^1H NMR spectrum in $\text{DMSO}-d_6$ for compound 5

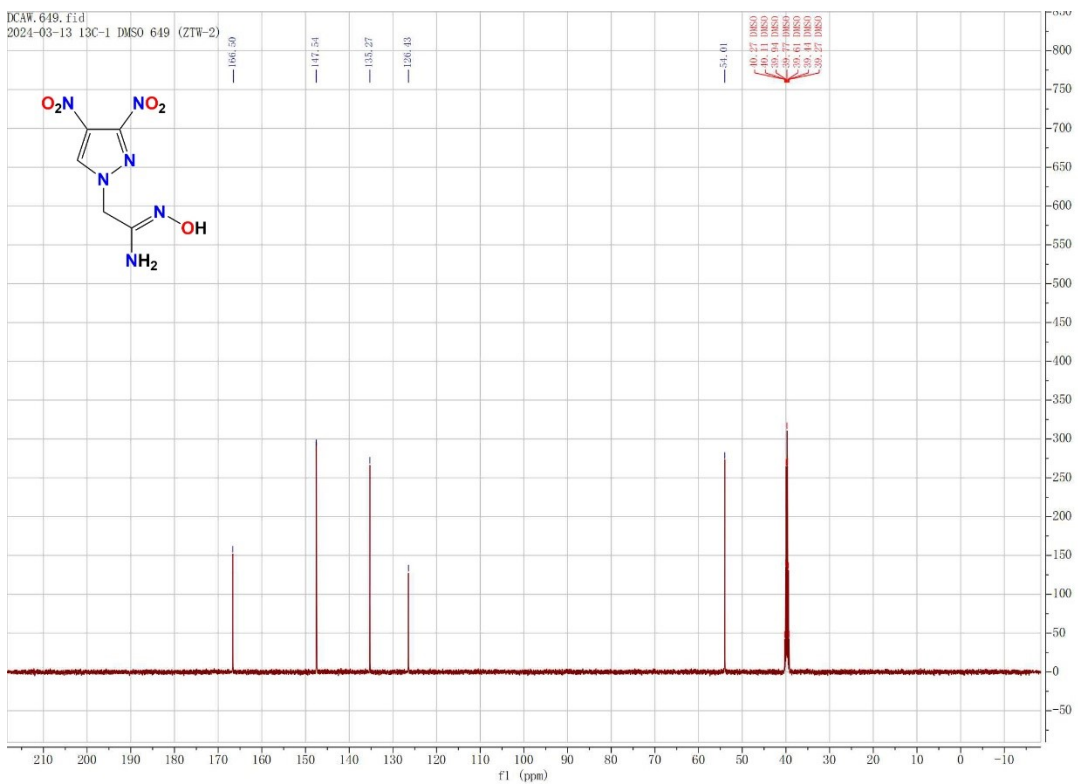


Figure S11. ^{13}C NMR spectrum in $\text{DMSO}-d_6$ for compound 5

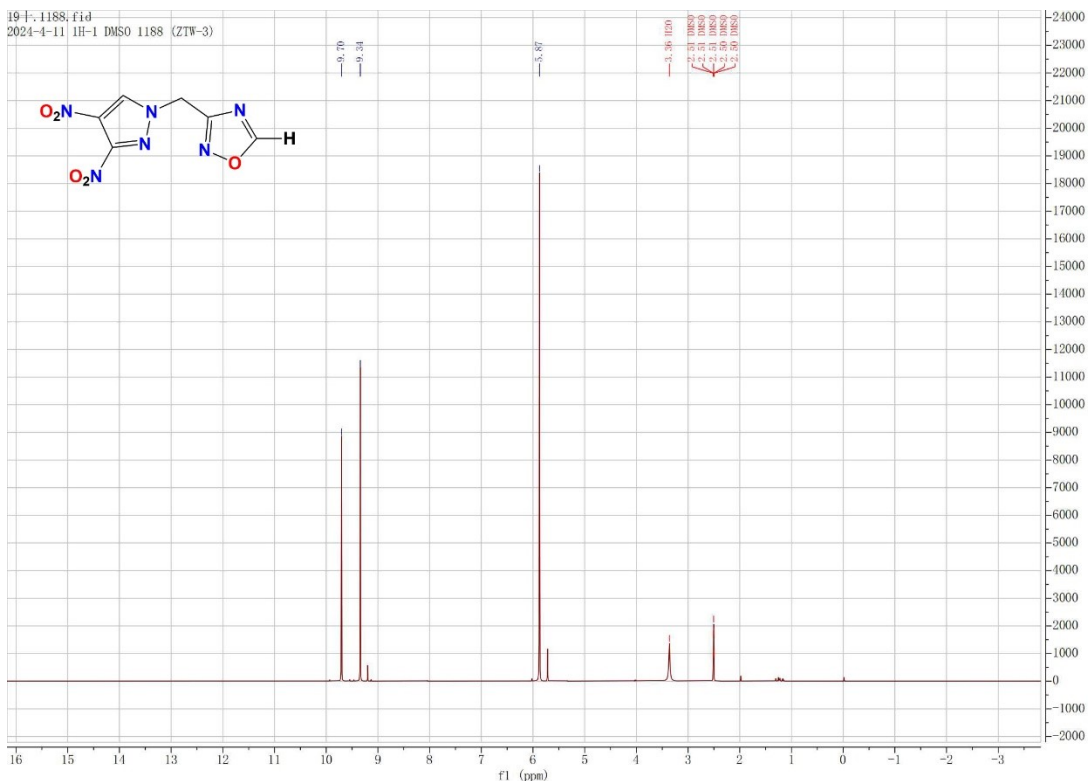


Figure S12. ^1H NMR spectrum in $\text{DMSO}-d_6$ for compound **6**

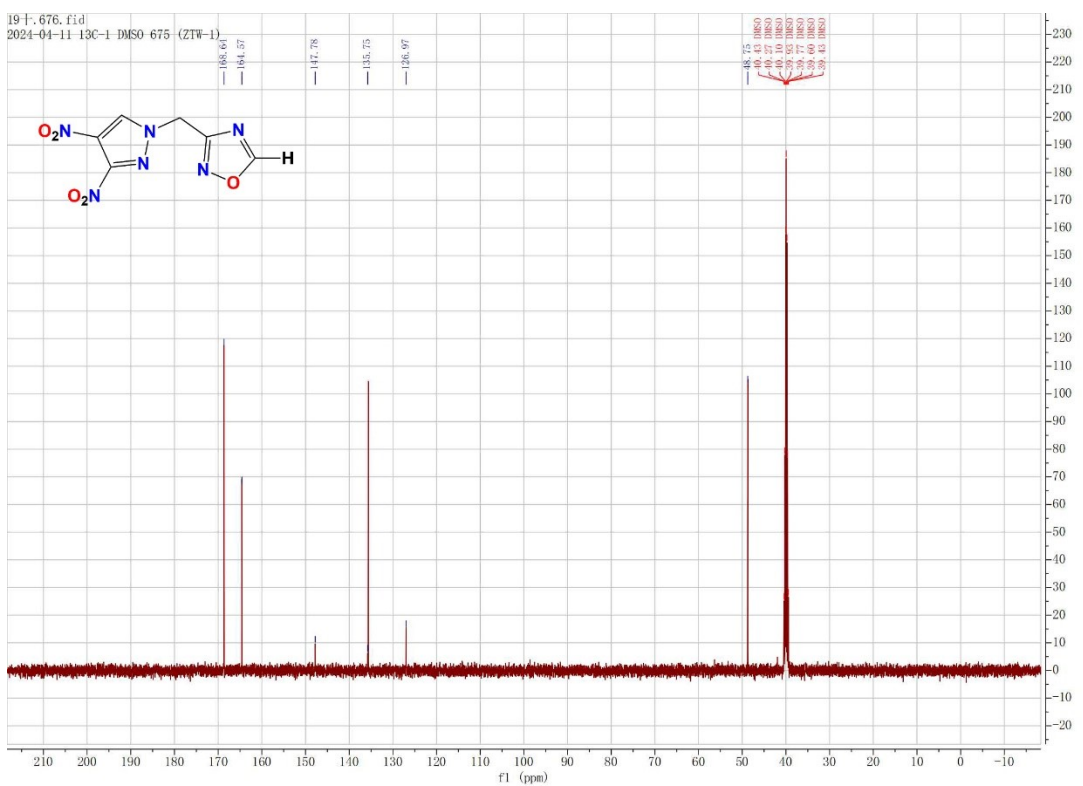


Figure S13. ^{13}C NMR spectrum in $\text{DMSO}-d_6$ for compound 6

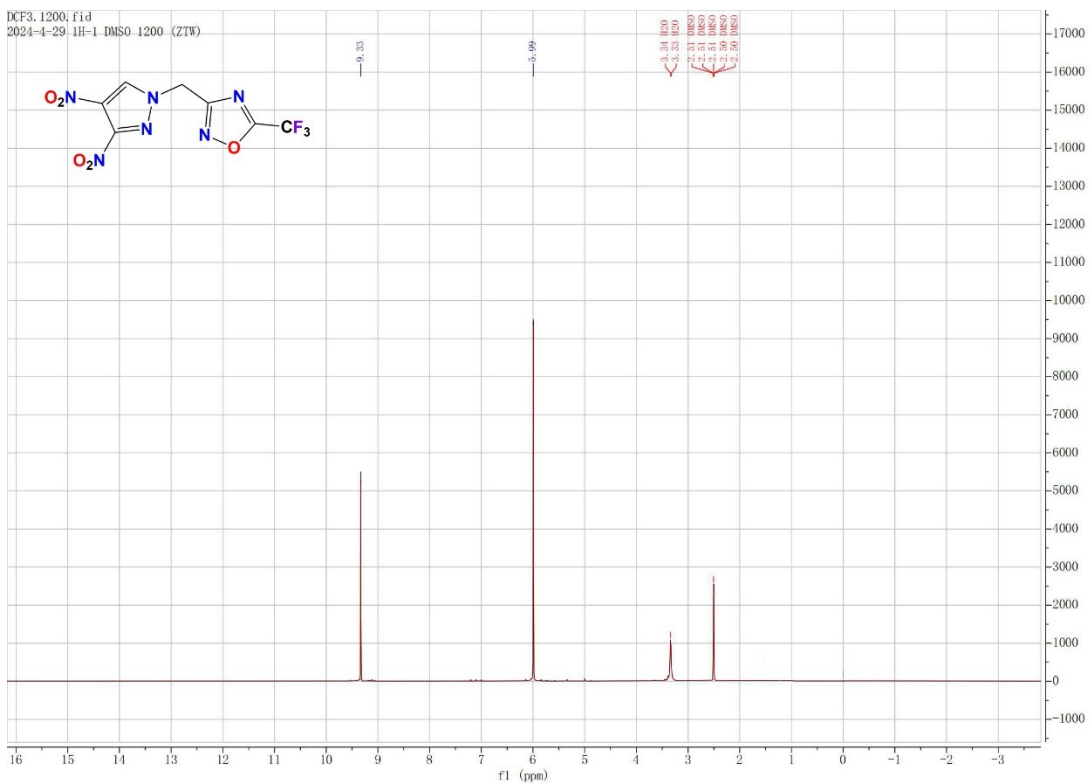


Figure S14. ^1H NMR spectrum in $\text{DMSO}-d_6$ for compound 7

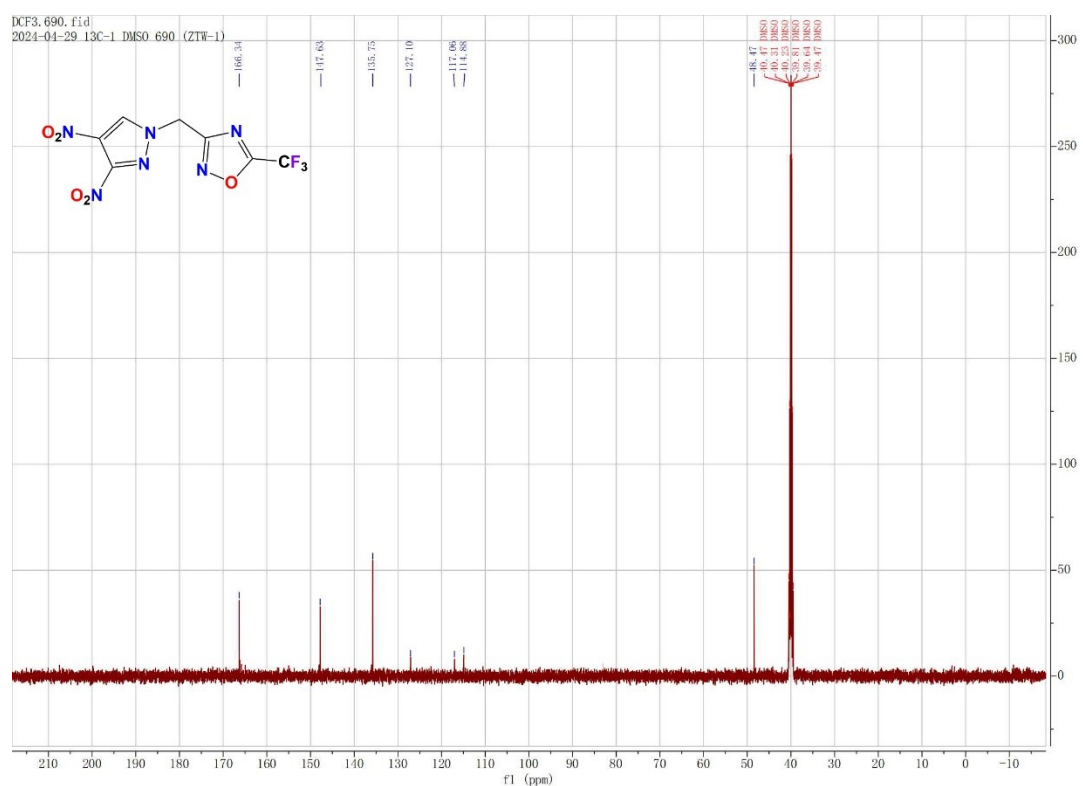


Figure S15. ^{13}C NMR spectrum in $\text{DMSO}-d_6$ for compound 7